Version of Record: https://www.sciencedirect.com/science/article/pii/S0921452620307377
Manuscript_1f5b8f5a6ca4f69f0f216b677e77281d

Enhancing the dielectric, electrocaloric and energy storage properties of lead-free $Ba_{0.85}Ca_{0.15}Zr_{0.1}Ti_{0.9}O_3$ ceramics prepared via sol-gel process

H. Mezzourh [1,2,*], S. Belkhadir [1], D. Mezzane [1,2], M. Amjoud [1], E. Choukri [1], A. Lahmar [2], Y. Gagou [2], Z. Kutnjak [3], M. El Marssi [2]

[1] Laboratory of Innovative Materials, Energy and Sustainable Development (IMED), Cadi-Ayyad University, Faculty of Sciences and Technology, BP 549, Marrakech, Morocco.

[2] Laboratory of Physics of Condensed Matter (LPMC), University of Picardie Jules Verne, Scientific Pole, 33 rue Saint-Leu, 80039 Amiens Cedex 1, France.

[3] Jozef Stefan Institute, Jamova Cesta 39, 1000 Ljubljana, Slovenia

*Corresponding author.

E-mail addresses: mezzourhhanane@gmail.com, hanane.mezzourh@ced.uca.ma

Abstract

The $Ba_{0.85}Ca_{0.15}Zr_{0.1}Ti_{0.9}O_3$ (BCZT) ceramics were successfully prepared by the sol-gel process and sintered at 1420°C. The effect of sintering times (2, 4 and 6 h) on structural, microstructural, electric properties, energy storage, and electrocaloric effect was systematically examined. X-ray diffraction (XRD) results show that all the samples crystallize in the pure perovskite structure. The morphotropic phase transition from the tetragonal to the orthorhombic phase (T-O) was identified and confirmed by Rietveld refinement. The BCZT ceramic sintered at 1420°C for 4h possesses a good relative density of 98% and exhibits optimal properties with a high dielectric permittivity ($\varepsilon_{r,max}$) ~16310, a large electrocaloric effect coefficient (ξ) ~ 0.244Kmm/kV and a high energy storage efficiency of 63.65%.

Keywords: BCZT ceramics; sol-gel method; dielectric; electrocaloric effect; energy storage.

© 2020 published by Elsevier. This manuscript is made available under the CC BY NC user license
https://creativecommons.org/licenses/by-nc/4.0/

1. Introduction

For many years, lead-based piezoelectric materials such as lead zirconium titanate $PbTiO_3$–$PbZrO_3$ (PZT) [1] , $Pb(MgNb)O_3$–$PbTiO_3$(PMN-PT), and $Pb(Ni_{1/3}Nb_{2/3})O_3$–$PbHfO_3$–$PbTiO_3$ (PNN–PHT) [2] are extensively used in various functional applications such as non-volatile memory, sensors, actuators, transducers, capacitors, generators, and energy harvesting devices, [3]–[6] due to their superior electrical performance close to the morphotropic phase boundaries. However, these compounds have the undeniable disadvantage of toxicity and volatility of lead. These materials have contributed to serious environmental and human health problems [7], [8]. Recently, many scientific teams have been searching for new eco-friendly alternative materials with advanced properties. By investigating various lead-free materials with perovskite structure (ABO_3) such as $BaTiO_3$(BT), $(Bi_{0.5}Na_{0.5})TiO_3$-$BaTiO_3$(BNT-BT), $(K_{0.5}Na_{0.5})NbO_3$ (KNN) and $Ba_{1-x}Ca_xTi_{1-y}ZryO_3$ (BCZT) [9]–[11]. Among of all the above materials, barium calcium zirconate titanate ($(Ba,Ca)(Zr,Ti)O_3$, BCZT) exhibits a super large piezoelectric coefficient (d_{33}) up to 620 pC/N [12] in a bulk ceramic with a perovskite structure, and possesses a high dielectric permittivity value of ~ 17184 [13] as well as important ferroelectric properties and low loss tangent (tan δ). It is thought that the high-performance of BCZT ceramics may stem from the morphotropic phase boundary that is a region of specific interest for electroceramic materials [14]. It is well known that, the chemical and electrical properties of electroceramics depend strongly on the synthesis methods and preparation conditions. Several synthesis techniques were employed to prepare perovskite powders such as solid-state technique, hydro-solvothermal synthesis and sol-gel process [15]–[18]. Many papers have reported that the sol-gel method provides a better homogeneity, chemical purity, and stoichiometric composition of the resultant phase comparing to the ceramics prepared by the solid-state method [19]. In general, the sintering factors such as temperature and dwelling time affect the structural and electrical properties of

BCZT ceramics [20], [21]. Cai et al. reported that excellent ferroelectric properties (2Pr = 31.62 μC/cm^2, 2Ec = 3.46 kV/cm) of $Ba_{0.85}Ca_{0.15}Zr_{0.1}Ti_{0.9}O_3$ ceramics obtained by sol-gel method, can be achieved by sintered at 1500 °C for 10h [22]. Moreover, an interesting recoverable energy density value of 0.52 J/cm^3 reported in $Ba_{0.85}Ca_{0.15}Zr_{0.1}Ti_{0.9}O_3$ by Wang et al. [19] indicates this ceramic could be a promising candidate for energy storage applications. Conversely, Rui Liu et al. found that the ceramic sintered at 1420°C exhibits a good dielectric permittivity with a weak dielectric loss ~ 0.015 [23], [24]. In that regard, our group has reported that BCZT-spherical nanoparticles and BCZT-rod-like ceramics elaborated by surfactant-assisted solvothermal route exhibit enhanced dielectric, ferroelectric and electrocaloric properties [25]. We have also studied the influence of the sintering temperature on the microstructure, dielectric, and diffusivity of the BCZT ceramic prepared by the sol-gel method [26]. In the present work, we investigate the effect of sintering dwell time at 1420°C on the dielectric, electrocaloric and energy storage properties of BCZT ceramics prepared by sol-gel technique.

2. Experimental details

2.1. Chemicals

For the preparation of BCZT ceramics, the following materials purchased from Sigma-Aldrich and Alfa Aesar were used: barium acetate $Ba(CH_3COO)_2$, calcium nitrate tetrahydrate $Ca(NO_3)_2.4H_2O$, titanium (IV) isopropoxide $Ti[OCH(CH_3)_2]_4$ and zirconium (IV) oxychloride octahydrate $ZrOCl_2.8H_2O$ as the starting materials, acetic acid and 2-Methoxyethanol were used as the solvents.

2.2. Synthesis procedure

The $Ba_{0.85}Ca_{0.15}Zr_{0.1}Ti_{0.9}O_3$ (BCZT) ceramic was synthesized by the sol-gel route. Firstly, the $Ba(CH_3COO)_2$ and $Ca(NO_3)_2.4H_2O$ were initially entirely dissolved in acetic acid according to the stoichiometric ratio under continuous stirring. Afterward, a stoichiometric amount of $ZrOCl_2.8H_2O$ was dissolved in 2-Methoxyethanol solution, then $Ti[OCH(CH_3)_2]_4$ was added and stirred. In the next step, this solution was added to the above (Ba, Ca) precursor solution and stirred for 1h at room temperature to yield a clear transparent BCZT solution. The pH was adjusted with ammonia to 6. The obtained sol was dried at 120°C for 24 h to eliminate the solvents and then grounded to a fine powder in a mortar. The powder was calcined for 4 h at 1000 °C in the air to form a pure crystalline phase. The calcined powder was then pressed into cylindrical disks with a diameter of 13 mm by uniaxial pressing under 100 MPa. Finally, the pellets were sintered at 1420 °C in an air atmosphere for 2, 4 and 6h and designated BCZT-t, where t is the sintering dwell time.

2.3. Characterization equipment

The sintered ceramics' phase structure was determined by X-ray diffraction (XRD, Panalytical X-Pert Pro) analysis using the Cu-Kα radiation with λ~1.540598 Å. The measurements were performed at room temperature in a range from 20° to 80° with a step size of 0.02°. Rietveld refinement analysis was achieved by using FullProf software.

The surfaces' morphologies were revealed by a Scanning Electron Microscope (SEM, Philips XL30) and (SEM, VEGA 3-Tscan) in association with energy dispersive X-ray (EDX) analysis. The densities of the pellets were measured using the Archimedes method [11]. The dielectric measurements and the impedance spectroscopy were examined using an HP 4284A precision impedance meter, controlled by a computer in the 20Hz to 1MHz frequency range. The sintered samples surfaces were covered with a conductive silver paste serving as electrodes for electrical measurements. The polarization-electric field (P-E) hysteresis loops

were collected using a commercial ferroelectric test system (TF Analyzer 3000, aixACCT). The electrocaloric adiabatic temperature variation (ΔT) and responsivity (ζ) were achieved by the indirect method from recorded (P-E) hysteresis loops at 1 Hz as a function of temperature.

3. Results and discussion

3.1. Structural analysis

Figure.1 presents the X-ray diffraction patterns of BCZT ceramics sintered for various dwell times. All samples exhibit pure perovskite structure without any secondary phase in the limit of device detection, suggesting that Ca^{2+} and Zr^{4+} have diffused into the $BaTiO_3$ lattice to form a solid solution [27]. To find out the phase structure of BCZT ceramics fabricated in different sintering times, fine scanning XRD patterns around 45° and 66° and Rietveld refinement of crystal structure were carried out. In general, the diffraction peaks of barium titanate around 45° may correspond to (002)/(200)T of the tetragonal phase, (200)/(220)O of the orthorhombic phase or (200)R of the rhombohedral phase [28]. It is observed from **Figure. 1.d** that the (200) peak splits into two diffraction peaks, which can be attributed to the tetragonal feature diffraction peaks of (002)T and (200)T, suggesting the presence of tetragonal phase. Furthermore, the formation of the triplet around 66° (**Figure. 1.e**) signifies the presence of the orthorhombic phase. According to the fitting results of diffraction peaks around 45° and 66° and the Rietveld refinement, it is concluded that the BCZT samples are the coexistence of O-T phase. Many reports are available with a coexistence phases at room temperature for the similar composition [29]–[31]. Structural information and phase composition are enlisted in **Table. 1**. The crystallite size was determined using Scherrer's formula [32] as following :

$$D = \frac{k \times \lambda}{\beta \times cos\theta} \ . \qquad (1)$$

Where k is the Scherrer constant, λ is the wavelength of the X-Rays used for the diffraction, β the « full width at half maximum » of the sharp peaks, and θ is the measured angle. From the **Table. 1**, it is observed that the crystallite size increases with increasing the dwell time, indicating better crystallinity for longer sintering time [33].

3.2. Microstructural and compositional analyses

Figure 2 displays the SEM images of the sintered BCZT ceramics' surface morphologies with different sintering times of 2, 4 and 6h (insets show the corresponding histograms). It can be seen that all the BCZT ceramics are densely sintered with irregular shaped and large grains up to micrometers. Furthermore, as shown in **Figure. 2a-c**. The average grain size estimated using analytical software (image J) has increased from 28 to 33 µm, increasing sintering time from 2h to 6h. The relative density of all studied samples is greater than 94 %. This could be attributed to the highly active and well dispersion precursor powder prepared by the sol-gel method [34]. Furthermore, it could be suggested that the sintering temperature of 1420°C was sufficient for the BCZT powder to produce good quality ceramics. The increase of relative density in BCZT-4h ceramic could be attributed to the proportion ratio of the coexistence tetragonal (T) and orthogonal (O) phases, which is higher when BCZT is sintered at 1420 °C for 4h as shown in **Table 1**. The relevant grain size distributions and relative densities estimated are listed in **Table. 1**.

In order to confirm the chemical composition of the BCZT ceramics, the EDX elemental analysis of the ceramics was determined as presented in **Figure. 3,** which indicates the presence of Ba, Ca, Ti, Zr, and O elements. It also gives Ba to Ca and Zr to Ti ratios as 5.38 and 9.67 respectively, which confirms the elemental stoichiometry of the as-prepared ceramic : as $Ba_{0.85}Ca_{0.15}Zr_{0.1}Ti_{0.9}O_3$. No other peak for any other element has been detected in the

spectrum, confirming the XRD observation and the chemical purity of the BCZT ceramics prepared by the sol-gel method.

3.3. Dielectric analysis

The temperature dependence of the relative dielectric permittivity (ε_r) and dielectric loss factor (tan δ) of BCZT ceramics measured from room temperature to 200 °C are shown in **Figure. 4.** Two dielectric anomalies were observed for all samples: the first one corresponds to the morphotropic phase transition from the orthorhombic to tetragonal (O-T) phase, with increasing sintering time T_{O-T} shifts from 31 to 24°C, while Tc shifts to higher temperature with increasing sintering time. The exact origin of this behavior is still unclear. The coexistence of the two phase structures in these ceramics may lead to good electrical properties. The dielectric permittivity maximum ($\varepsilon_{r,max}$) values depend significantly on sintering time, as shown in **Table. 2**. It is worth noting that the BCZT-4h exhibits the largest value of dielectric permittivity ($\varepsilon_{r,max} \approx 16310$, at 1 kHz), which is higher and/or similar to that obtained by other literature reported on BCZT ceramics prepared by different methods as illustrated in **Table. 3**. The significant improvement of the dielectric permittivity could be related to the high density of BCZT-4h [35]. All samples keep a low value of tan δ (≤ 0.06, at 1 kHz) which is probably attributed to the dense microstructure and the lower electron diffusion in the grain boundaries [36]. The overall properties (Tc, $\varepsilon_{r.max}$ $Tan\delta_{Tc}$) are recorded and summarized in **Table. 2**.

The temperature dependence of the dielectric permittivity for BCZT-4h ceramic at different frequencies, ranging from 100 Hz to 100 kHz, is illustrated in **Figure. 5**. The first derivative of relative permittivity as a function of temperature is plotted **(inset of Figure. 5)**. It is noticed that the dielectric maximum decreases as a function of frequency, decrease may be attributed to the reduction of net polarization due to the accumulation of space charges at the grain boundaries, which subsequently leads to the formation of interfacial polarization. In general,

as frequency increases, the net polarization decreases as each polarization mechanism ceases to contribute, and hence, its dielectric constant decreases [26], [37]. However, there is no frequency dispersion in T_C. These two behaviors are associated with the diffuse phase transition in all samples and differ from the relaxor materials [38].

It is known that the classical ferroelectrics follow the Curie-Weiss law above Curie temperature [39], which is defined by the following equation:

$$\frac{1}{\varepsilon_r} = \frac{T - T_0}{C} \ (T > T_0). \qquad (2)$$

Here, T_0 denotes the Curie–Weiss temperature and C is the Curie-Weiss constant.

The temperature-dependence of reciprocal dielectric permittivity at a frequency of 1kHz for BCZT-4h ceramic is presented in **Figure. 6**.

The values of the fitting results obtained by Eq. (2) are listed in the **Table. 2**. The Curie constant value for all samples is in the order of 10^5 K, which are accordant with typical displacive-type ferroelectric [40].

The changes of Curie-Weiss behavior (ΔT_m) indicate the deviation from the Curie-Weiss law and the degree of diffuseness [41], which can be defined by :

$$\Delta T_m = T_{cw} - T_m . \qquad (3)$$

where T_{cw} represents the temperature at which the dielectric permittivity begins to deviate from Curie-Weiss law, and T_m is the temperature at maximum dielectric permittivity.

It is found that ΔT_m values are 39.74, 40.89 and 39.93°C for sintering times of 2, 4 and 6h, respectively, which implies a weaker diffuse phase transition behavior [33].

A modified form of Curie-Weiss law [42], proposed by Uchino is used to describe the diffuseness phase transition:

$$\frac{1}{\varepsilon_r} - \frac{1}{\varepsilon_m} = \frac{(T - T_m)^\gamma}{C} \ (1 \leq \gamma \leq 2). \qquad (4)$$

where ε_r is the relative permittivity, ε_m is the maximum relative permittivity, T_m is the temperature of the maximum dielectric permittivity, C is the Curie–Weiss constant and γ is the degree of diffuse phase transition. Here parameter $1< \gamma <2$, gives information about the character of phase transition; $\gamma = 1$ corresponds to normal ferroelectrics, and $\gamma = 2$ corresponds to relaxor ferroelectrics. The inset in **Figure. 6** illustrates the linear fit plots of $\ln(1/\varepsilon_r - 1/\varepsilon_m)$ versus $\ln(T - T_m)$ at 1kHz for BCZT-4h ceramic, and the value of γ is obtained from of the fitting curves. The values of γ are 1.760, 1.792 and 1.783 for 2, 4 and 6h, respectively, which indicate an incomplete diffuse phase transition behavior [43].

3.4. Ferroelectric analysis

To assess the EC effect, P-E hysteresis loops shown in **Figure. 7** were registered for the BCZT-4h ceramic at different temperatures. It can be seen from the hysteresis loops that the increase of temperature decreases the ferroelectric properties, which is typical of the ferroelectric to the paraelectric phase transition.

The grain size, density, and phase homogeneity affect the Ec, Ps, Pr, and the hysteresis loops' squareness. For an ideal hysteresis loop, the squareness parameter is equal to 2. According to Haertling and Zimmer, the squareness of the P-E loops can be quantitatively calculated using the following equation [44], [45] :

$$R_{sq} = \frac{P_r}{P_s} + \frac{P_{1.1Ec}}{P_r} . \qquad (5)$$

Where R_{sq} is the squareness of the hysteresis loop, Ps is saturation polarization, Pr is remnant polarization, and $P_{1.1Ec}$ represents the polarization at an electric field equal to 1.1 times the coercive field (Ec). It can be seen that all samples exhibit approximately a value close to 2

(see **Table. 3**), indicating a better homogeneity and uniformity in grain size of the samples prepared by sol-gel, which contributes to a fast domain switching [46].

Figure. 8 displays the comparative (P-E) loops of polarization versus electric field of the sintered BCZT ceramics with various dwell time of 2, 4 and 6 h measured at room temperature under the critical electric field. It can be seen that the sintering dwell time has a significant effect on the ferroelectric properties (Ec, Ps, Pr) of BCZT ceramics. Indeed, the Ec of BCZT ceramics decreases from 2.3131 to 1.7427 kV/cm with an increase of dwell time from 2h to 6h, such low coercive fields (Ec) make the domain switching easier during the polarization reversal process and makes the samples ferroelectrically soft [47]. These values are lower and/or nearly the same as observed in other BCZT ceramics prepared by different processes and under various sintering conditions (see **Table. 3**). However, for BCZT-4h, Ps and Pr initially increase to a maximum value of 9.6955 and 6.8854 μC/cm^2, respectively, and then decrease as shown in **Table. 3**. The excellent ferroelectric properties of BCZT-4h can be attributed to its high relative density (>98%) and large grain size (30.79μm). It could be understood that the BCZT-4h possesses the critical grain size over which the electrical properties can be enhanced.

3.5. Energy storage performances

Generally, for nonlinear dielectrics, the recoverable energy density W_{rec}, total energy density W_{total}, and energy storage efficiency η can be determined from the polarization hysteresis (P-E) loops using the following equations [48]:

$$Wtotal = \int_{0}^{Pmax} EdP \qquad (6)$$

$$Wrec = \int_{Pr}^{Pmax} EdP \qquad (7)$$

and

$$\eta = \frac{Wrec}{Wtotal} \times 100\,. \qquad (8)$$

Pmax, Pr, E, Wtotal, Wrec and η refer to maximum polarization, remnant polarization, applied external electric field strength, energy storage density, recoverable energy density, and energy storage efficiency. **Figure. 10** shows the variation of W_{rec}, W_{loss} and η for BCZT ceramics as a function of sintering time. The BCZT-4h ceramic showed better recoverable energy density (green area in **Figure. 9**) W_{rec} (10.61 mJ/cm^3 at ~ 7.77 kV/cm). This improvement of W_{rec} may be due to the large Ps values and low Ec values, which facilitate the reorientation of dipoles with low electrical field. The values of efficiency (η) of the samples are relatively comparable with others previously reported in the literature under a strong electric field (see **Table. 4**). The best value of efficiency is η=63.65% at 140°C under an electric field of ~7.77 kV/cm, which is relatively comparable with others reported in the literature under a strong electric field. In practical applications, a efficient energy storage material not only requires a high energy density, but also a high thermal stability or energy storage variation (ESV) that could be calculated by the following equation [49]:

$$\frac{\Delta W_{rec,T}}{W_{rec,300K}} = \left|\frac{W_{rec,T} - W_{rec,300K}}{W_{rec,300K}}\right|. \qquad (9)$$

Where $W_{rec,T}$ is the W_{rec} value at a given temperature, and $\Delta W_{rec,T}$ is the difference of $W_{rec,T}$ and $W_{rec,300\ K}$. It is worth noting that the BCZT-4h exhibits the smallest ESV value which is less than 19.87% in the temperature range from 300 to 350 K. The energy-storage variation in as-prepared ceramics is close to that reported by Z.Hanani et al. for the BCZT ceramic with the same composition [49]. Moreover, the obtained values of ESV are lower than that found by Jayakrishnan et al. in $0.6BaZr_{0.20}Ti_{0.80}O_3$–$0.4Ba_{0.70}Ca_{0.30}TiO_3$ [50].

3.6. Indirect electrocaloric measurements

Using Maxwell relation $(\frac{\partial P}{\partial T})_E = (\frac{\partial S}{\partial E})_T$ the adiabatic temperature change ΔT under an applied electric field is calculated by the following equation [51]:

$$\Delta T = -\frac{1}{\rho}\int_{E2}^{E1} \frac{T}{Cp}(\frac{\partial P}{\partial T})_E \, dE \ . \qquad (10)$$

where ρ is the density of the ceramics, E1 and E2 are the lower and higher electric field limits, respectively, Cp denotes the specific heat capacity of the ceramics.

Several factors can influence the performance of the electrocaloric materials; the nature of the phase transition is one of these factors. Two types of transitions can be distinguished; first-order transition is associated with a high value of ΔT with a restricted temperature range around Tc, while the second-order transition is generally characterized by a low electrocaloric effect with a broad temperature range around Tc [52].

The electrocaloric (EC) properties of the fabricated BCZT ceramics for an applied electric field 6 kV/cm are shown in **Figure. 11**. The BCZT-4h and BCZT-6h present high values of $\Delta T_{EC,max}$ (0.1467K and 0.1513K respectively) in a limited temperature ranges; this may be related to the increase of the spontaneous polarization. This behavior indicates that the phase transition is of the first order. However, BCZT-2h presents a very low value of $\Delta T_{EC,max}$ with a relatively broad temperature range ($FWHM_{\Delta T}$) of ≈ 56K, which indicates that the transition is of second order.

The EC responsivity (ξ=ΔT/ΔE) values obtained for the BCZT samples are enlisted in **Table. 5**, comparing with different studies reported in the literature. We notice that the BCZT ceramics sintered at 4h and 6h exhibit high EC responsivity of 0.244 K mm/kV and 0.252 K mm/kV respectively at a low applied electric field of 6 kV/cm. These values appear to be comparable and/or higher than those of the BCZT ceramics prepared by solid-state and sol-gel

routes (see **Table. 5**). It is worth mentioning that the most important criteria that have to be considered during the development of EC materials is the fact that the EC responsivity ($\Delta T/\Delta E$) should be as high as possible within a broad interval of temperature [53]. The BCZT-4h exhibits a better EC responsivity with a relatively large temperature interval ($FWHM_{\Delta T}$) of $\approx$ 33K.

4. Conclusion

In this contribution, we have dealt with the effect of sintering time on the structural, dielectric, ferroelectric, and piezoelectric properties of lead-free $Ba_{0.85}Ca_{0.15}Ti_{0.9}Zr_{0.1}O_3$ (BCZT) ceramics prepared by sol-gel route. BCZT ceramic fabricated at 1420 °C for 4h with a relative density of 98% has demonstrated simultaneously enhanced dielectric properties around the MPB region, i.e., $\varepsilon_{r.max}$ = 16310 and improved electrocaloric effect; ζ = 0.244 K mm/kV. Besides, BCZT-4h displayed a relatively high Wrec of 10.61 mJ/cm^3 with an efficiency coefficient of ~ 63% at low electric field strength. These results suggest that the synthesized BCZT-4h ceramic could be a promising candidate for electrocaloric and energy storage applications.

Acknowledgements

The authors gratefully acknowledge the financial support of CNRST Priority Program PPR 15/2015 and the European H2020-MSCA-RISE-2017-ENGIMA action.

References

[1] Z. Sun *et al.*, « Dielectric and piezoelectric properties and PTC behavior of $Ba_{0.9}Ca_{0.1}Ti_{0.9}Zr_{0.1}O_3$−xLa ceramics prepared by hydrothermal method », *Materials Letters*, vol. 118, p. 1-4, mars 2014, doi: 10.1016/j.matlet.2013.12.043.

[2] R. Bhimireddi, B. Ponraj, et K. B. R. Varma, « Structural, Optical, and Piezoelectric Response of Lead-Free Ba $_{0.95}$ Mg $_{0.05}$ Zr $_{0.1}$ Ti $_{0.9}$ O $_3$ Nanocrystalline Powder », *J. Am. Ceram. Soc.*, vol. 99, n° 3, p. 896-904, mars 2016, doi: 10.1111/jace.14018.

[3] S. Saparjya, T. Badapanda, S. Behera, B. Behera, et P. R. Das, « Effect of Gadolinium on the structural and dielectric properties of BCZT ceramics », *Phase Transitions*, vol. 93, n° 2, p. 245-262, févr. 2020, doi: 10.1080/01411594.2020.1711905.

[4] S. D. Chavan et D. J. Salunkhe, « Ferroelectric Relaxation Behavior of Lead free BCZT Ceramics », vol. 3, n° 11, p. 5, 2012.

[5] J. Tao, Z. Yi, Y. Liu, M. Zhang, et J. Zhai, « Dielectric Tunability, Dielectric Relaxation, and Impedance Spectroscopic Studies on (Ba $_{0.85}$ Ca $_{0.15}$)(Ti $_{0.9}$ Zr $_{0.1}$)O $_3$ Lead-Free Ceramics », *J. Am. Ceram. Soc.*, vol. 96, n° 6, p. 1847-1851, juin 2013, doi: 10.1111/jace.12265.

[6] S. Ben Moumen *et al.*, « Impedance spectroscopy studies on lead free Ba 1-x Mg x (Ti $_{0.9}$ Zr $_{0.1}$)O $_3$ ceramics », *Superlattices and Microstructures*, vol. 118, p. 45-54, juin 2018, doi: 10.1016/j.spmi.2018.04.012.

[7] W. Cai *et al.*, « Synergistic effect of grain size and phase boundary on energy storage performance and electric properties of BCZT ceramics », *J Mater Sci: Mater Electron*, avr. 2020, doi: 10.1007/s10854-020-03446-z.

[8] S. Ben Moumen *et al.*, « Structural, Dielectric, and Magnetic Properties of Multiferroic ($1 - x$) La $_{0.5}$ Ca $_{0.5}$ MnO $_3$ -(x) BaTi $_{0.8}$ Sn $_{0.2}$ O $_3$ Laminated Composites », *IEEE*

Trans. Ultrason., Ferroelect., Freq. Contr., vol. 66, n° 12, p. 1935-1941, déc. 2019, doi: 10.1109/TUFFC.2019.2935459.

[9] P. Jaimeewong, M. Promsawat, A. Watcharapasorn, et S. Jiansirisomboon, « Comparative study of properties of BCZT ceramics prepared from conventional and sol-gel auto combustion powders », *Integrated Ferroelectrics*, vol. 175, n° 1, p. 25-32, oct. 2016, doi: 10.1080/10584587.2016.1199913.

[10] J. Hao, W. Bai, W. Li, et J. Zhai, « Correlation Between the Microstructure and Electrical Properties in High-Performance $(Ba_{0.85}Ca_{0.15})(Zr_{0.1}Ti_{0.9})O_3$ Lead-Free Piezoelectric Ceramics », *J. Am. Ceram. Soc.*, vol. 95, n° 6, p. 1998-2006, juin 2012, doi: 10.1111/j.1551-2916.2012.05146.x.

[11] N. Buatip *et al.*, « Investigation on electrical properties of BCZT ferroelectric ceramics prepared at various sintering conditions », *Integrated Ferroelectrics*, vol. 187, n° 1, p. 45-52, févr. 2018, doi: 10.1080/10584587.2018.1445395.

[12] S.-W. Zhang, H. Zhang, B.-P. Zhang, et S. Yang, « Phase-transition behavior and piezoelectric properties of lead-free $(Ba_{0.95}Ca_{0.05})(Ti_{1-x}Zr_x)O_3$ ceramics », *Journal of Alloys and Compounds*, vol. 506, n° 1, p. 131-135, sept. 2010, doi: 10.1016/j.jallcom.2010.06.157.

[13] P. Yong, D. Shihua, N. Wenju, X. Qin, et W. Xiaoliang, « Dielectric Properties and Relaxor Behavior of Nd Doping BCZT Ceramics », *Ferroelectrics*, vol. 450, n° 1, p. 21-27, janv. 2013, doi: 10.1080/00150193.2013.838459.

[14] Y. Tian, Y. Gong, D. Meng, H. Deng, et B. Kuang, « Low-temperature sintering and electric properties of BCT–BZT and BCZT lead-free ceramics », *J Mater Sci: Mater Electron*, vol. 26, n° 6, p. 3750-3756, juin 2015, doi: 10.1007/s10854-015-2898-2.

[15] A. Thongtha, K. Angsukased, N. Riyamongkol, et T. Bongkarn, « Preparation of ($Ba_{1-x}Sr_x$)(Zr_xTi_{1-x})O_3 Ceramics via the Solid State Reaction Method », *Ferroelectrics*, vol. 403, n° 1, p. 68-75, oct. 2010, doi: 10.1080/00150191003748907.

[16] M. Iranmanesh, M. Lingg, M. Stir, et J. Hulliger, « Sol gel and ceramic synthesis of $Sr_2FeMo_{1-x}W_xO_6$ ($0 \leq x \leq 1$) double perovskites series », *RSC Adv.*, vol. 6, n° 48, p. 42069-42075, 2016, doi: 10.1039/C6RA03923E.

[17] M. Ito, M. Hagiwara, et S. Fujihara, « Hydrothermal synthesis of lead-free perovskite $(Bi_{1/2}K_{1/2})(Zr_xTi_{1-x})O_3$ powders », *J. Ceram. Soc. Japan*, vol. 125, n° 6, p. 454-457, 2017, doi: 10.2109/jcersj2.16263.

[18] T. Kimijima, K. Kanie, M. Nakaya, et A. Muramatsu, « Solvothermal Synthesis of Shape-Controlled Perovskite $MTiO_3$ (M = Ba, Sr, and Ca) Particles in H_2O/Polyols Mixed Solutions », *Mater. Trans.*, vol. 55, n° 1, p. 147-153, 2014, doi: 10.2320/matertrans.M2013350.

[19] Z. Wang *et al.*, « Synthesis, structure, dielectric, piezoelectric, and energy storage performance of $(Ba_{0.85}Ca_{0.15})(Ti_{0.9}Zr_{0.1})O_3$ ceramics prepared by different methods », *J Mater Sci: Mater Electron*, vol. 27, n° 5, p. 5047-5058, mai 2016, doi: 10.1007/s10854-016-4392-x.

[20] Y. P. Jiang, X. G. Tang, S. G. Ju, Q. X. Liu, T. F. Zhang, et H. F. Xiong, « Influence of sintering temperature on the ferroelectric and piezoelectric properties of $(Ba_{0.85}Ca_{0.15})(Zr_{0.1}Ti_{0.9})O_3$ ceramics », *J Mater Sci: Mater Electron*, vol. 27, n° 3, p. 3048-3052, mars 2016, doi: 10.1007/s10854-015-4128-3.

[21] J. Wu, D. Xiao, W. Wu, J. Zhu, et J. Wang, « Effect of dwell time during sintering on piezoelectric properties of $(Ba_{0.85}Ca_{0.15})(Ti_{0.90}Zr_{0.10})O_3$ lead-free ceramics », *Journal of Alloys and Compounds*, vol. 509, n° 41, p. L359-L361, oct. 2011, doi: 10.1016/j.jallcom.2011.08.024.

[22] W. Cai *et al.*, « Effects of oxygen partial pressure on the electrical properties and phase transitions in (Ba,Ca)(Ti,Zr)O_3 ceramics », *J Mater Sci*, vol. 55, n° 23, p. 9972-9992, août 2020, doi: 10.1007/s10853-020-04771-8.

[23] R. Liu, Y. Qiao, X. Zhang, et C.-X. Lu, « Effects of calcination temperatures on the morphology, architecture and dielectric properties of BCZT ceramics », *Bull Mater Sci*, vol. 42, n° 4, p. 140, août 2019, doi: 10.1007/s12034-019-1825-1.

[24] R. Liu, « Sol-gel Synthesis of $(Ba_{0.85}Ca_{0.15})(Zr_{0.1}Ti_{0.9})O_3$ Ceramics and their Dielectric Temperature Properties », p. 3.

[25] Z. Hanani *et al.*, « Enhanced dielectric and electrocaloric properties in lead-free rod-like BCZT ceramics », *J Adv Ceram*, vol. 9, n° 2, p. 210-219, avr. 2020, doi: 10.1007/s40145-020-0361-1.

[26] S. Belkhadir *et al.*, « Impedance spectroscopy analysis of the diffuse phase transition in lead-free $(Ba_{0,85}Ca_{0,15})(Zr_{0.1}Ti_{0.9})O_3$ ceramic elaborated by sol-gel method », *Superlattices and Microstructures*, vol. 127, p. 71-79, mars 2019, doi: 10.1016/j.spmi.2018.03.009.

[27] S. S. Mane et D. J. Salunkhe, « Structural and Dielectric Investigations on $x[Ba_{0.7}Ca_{0.3}TiO_3]$-$(1-x)[BaZr_{0.2}Ti_{0.8}O_3]$ Lead-Free Mixed Ceramic Compositions », vol. 4, n° 2, p. 6, 2013.

[28] I. Coondoo *et al.*, « A comparative study of structural and electrical properties in lead-free BCZT ceramics: Influence of the synthesis method », *Acta Materialia*, vol. 155, p. 331-342, août 2018, doi: 10.1016/j.actamat.2018.05.029.

[29] Y. Tian, L. Wei, X. Chao, Z. Liu, et Z. Yang, « Phase Transition Behavior and Large Piezoelectricity Near the Morphotropic Phase Boundary of Lead-Free $(Ba_{0.85}Ca_{0.15})(Zr_{0.1}Ti_{0.9})O_3$ Ceramics », *J. Am. Ceram. Soc.*, vol. 96, n° 2, p. 496-502, févr. 2013, doi: 10.1111/jace.12049.

[30] W. Cai *et al.*, « Effects of oxygen partial pressure on the electrical properties and phase transitions in (Ba,Ca)(Ti,Zr)O3 ceramics », *J Mater Sci*, vol. 55, n° 23, p. 9972-9992, août 2020, doi: 10.1007/s10853-020-04771-8.

[31] Q. Zhang *et al.*, « Enhanced piezoelectric response of (Ba,Ca)(Ti, Zr)O_3 ceramics by super large grain size and construction of phase boundary », *Journal of Alloys and Compounds*, vol. 794, p. 542-552, juill. 2019, doi: 10.1016/j.jallcom.2019.04.247.

[32] R. Jacob, H. G. Nair, et J. Isac, « Structural and Morphological Studies of Nanocrystalline Ceramic $BaSr_{0.9}Fe_{0.1}TiO_4$ », *ILCPA*, vol. 41, p. 100-117, nov. 2014, doi: 10.18052/www.scipress.com/ILCPA.41.100.

[33] X. Ji *et al.*, « Structural and electrical properties of BCZT ceramics synthesized by sol–gel-hydrothermal process at low temperature », *J Mater Sci: Mater Electron*, vol. 30, n° 13, p. 12197-12203, juill. 2019, doi: 10.1007/s10854-019-01578-5.

[34] A. Mirzaei, M. Bonyani, et S. Torkian, « Synthesis and characterization of nanocrystalline PZT powders: From sol to dense ceramics », *PAC*, vol. 10, n° 1, p. 9-16, 2016, doi: 10.2298/PAC1601009M.

[35] P. Parjansri, U. Intatha, K. Pengpat, et S. Eitssayeam, « Improvement in the electrical properties of BCZT Ceramics induced by self-seeds », *Appl. Phys. A*, vol. 125, n° 6, p. 421, juin 2019, doi: 10.1007/s00339-019-2711-9.

[36] Y. Tian, Y. Gong, Z. Zhang, et D. Meng, « Phase evolutions and electric properties of BaTiO3 ceramics by a low-temperature sintering process », *J Mater Sci: Mater Electron*, vol. 25, n° 12, p. 5467-5474, déc. 2014, doi: 10.1007/s10854-014-2330-3.

[37] Ch. Rayssi, S. El.Kossi, J. Dhahri, et K. Khirouni, « Frequency and temperature-dependence of dielectric permittivity and electric modulus studies of the solid solution $Ca_{0.85}Er_{0.1}Ti_{1-x}Co_{4x/3}O_3$ ($0 \leq x \leq 0.1$) », *RSC Adv.*, vol. 8, n° 31, p. 17139-17150, 2018, doi: 10.1039/C8RA00794B.

[38] S. Mitra, A. R. Kulkarni, et O. Prakash, « Diffuse phase transition and electrical properties of lead-free piezoelectric ($Li_x Na_{1-x}$)NbO_3 ($0.04 \leq x \leq 0.20$) ceramics near morphotropic phase boundary », *Journal of Applied Physics*, vol. 114, n° 6, p. 064106, août 2013, doi: 10.1063/1.4817815.

[39] P. Bharathi et K. B. R. Varma, « Grain and the concomitant ferroelectric domain size dependent physical properties of $Ba_{0.85} Ca_{0.15} Zr_{0.1} Ti_{0.9} O_3$ ceramics fabricated using powders derived from oxalate precursor route », *Journal of Applied Physics*, vol. 116, n° 16, p. 164107, oct. 2014, doi: 10.1063/1.4900494.

[40] R. Yevych, M. Medulych, et Y. Vysochanskii, « Nonlinear dynamics of ferroelectrics with three-well local potential », *Condens. Matter Phys.*, vol. 21, n° 2, p. 23001, juin 2018, doi: 10.5488/CMP.21.23001.

[41] S. Hunpratub, S. Maensiri, et P. Chindaprasirt, « Synthesis and characterization of $Ba_{0.85}Ca_{0.15}Ti_{0.9}Zr_{0.1}O_3$ ceramics by hydrothermal method », *Ceramics International*, vol. 40, n° 8, p. 13025-13031, sept. 2014, doi: 10.1016/j.ceramint.2014.04.166.

[42] I. Coondoo, N. Panwar, H. Amorín, M. Alguero, et A. L. Kholkin, « Synthesis and characterization of lead-free $0.5Ba(Zr_{0.2} Ti_{0.8})O_3$ -$0.5(Ba_{0.7} Ca_{0.3})TiO_3$ ceramic », *Journal of Applied Physics*, vol. 113, n° 21, p. 214107, juin 2013, doi: 10.1063/1.4808338.

[43] A. Belboukhari *et al.*, « Studies of Diffuse Phase Transition in Ferroelectric Solid Solution $Pb_{1-x} K_{2x} Nb_2 O_6$ (x = 0.1, 0.2, 0.25 and 0.3) », *Ferroelectrics*, vol. 444, n° 1, p. 116-124, janv. 2013, doi: 10.1080/00150193.2013.786619.

[44] M. Q. Awan, J. Ahmad, L. Norén, T. Lu, et Y. Liu, « Structure, dielectric and ferroelectric properties of lead free $(K,Na)(Nb)O_3$-$xBiErO_3$ piezoelectric ceramics », *J Mater Sci: Mater Electron*, vol. 29, n° 9, p. 7142-7151, mai 2018, doi: 10.1007/s10854-018-8702-3.

[45] W. Janbua, T. Bongkarn, T. Kolodiazhnyi, et N. Vittayakorn, « High piezoelectric response and polymorphic phase region in the lead-free piezoelectric $BaTiO_3$ –$CaTiO_3$ –$BaSnO_3$ ternary system », *RSC Adv.*, vol. 7, n° 48, p. 30166-30176, 2017, doi: 10.1039/C7RA04017B.

[46] A. Khesro *et al.*, « Temperature Dependent Piezoelectric Properties of Lead-Free (1-x)$K_{0.6}Na_{0.4}NbO_3$–x$BiFeO_3$ Ceramics », *Front. Mater.*, vol. 7, p. 140, mai 2020, doi: 10.3389/fmats.2020.00140.

[47] E. Chandrakala, J. Paul Praveen, B. K. Hazra, et D. Das, « Effect of sintering temperature on structural, dielectric, piezoelectric and ferroelectric properties of sol–gel derived BZT-BCT ceramics », *Ceramics International*, vol. 42, n° 4, p. 4964-4977, mars 2016, doi: 10.1016/j.ceramint.2015.12.009.

[48] H. Yang, F. Yan, Y. Lin, et T. Wang, « Novel Strontium Titanate-Based Lead-Free Ceramics for High-Energy Storage Applications », *ACS Sustainable Chem. Eng.*, vol. 5, n° 11, p. 10215-10222, nov. 2017, doi: 10.1021/acssuschemeng.7b02203.

[49] Z. Hanani, « Thermally-stable high energy storage performances and large electrocaloric effect over a broad temperature span in lead-free BCZT ceramic », *RSC Advances*, p. 10, 2020.

[50] A. R. Jayakrishnan *et al.*, « Composition-dependent x$Ba(Zr_{0.2}Ti_{0.8})O_3$-(1-x)$(Ba_{0.7}Ca_{0.3})TiO_3$ bulk ceramics for high energy storage applications », *Ceramics International*, vol. 45, n° 5, p. 5808-5818, avr. 2019, doi: 10.1016/j.ceramint.2018.11.250.

[51] A. Bauzá, T. J. Mooibroek, et A. Frontera, « Towards design strategies for anion–π interactions in crystal engineering », *CrystEngComm*, vol. 18, n° 1, p. 10-23, 2016, doi: 10.1039/C5CE01813G.

[52] D. Li et S.-G. Lu, « Electrocaloric Effect and Phase Transitions in Ferroelectrics », *Int J Metall Mater Eng*, vol. 4, n° 1, avr. 2018, doi: 10.15344/2455-2372/2018/141.

[53] H. Kaddoussi, A. Lahmar, Y. Gagou, J.-L. Dellis, H. Khemakhem, et M. E. Marssi, « Electro-caloric effect in lead-free ferroelectric Ba1−Ca $(Zr_{0.1}Ti_{0.9})_{0.925}$ $Sn_{0.075}O_3$ ceramics », *Ceramics International*, vol. 41, n° 10, p. 15103-15110, déc. 2015, doi: 10.1016/j.ceramint.2015.08.080.

[54] X. Ji *et al.*, « Structural and electrical properties of BCZT ceramics synthesized by sol–gel process », *J Mater Sci: Mater Electron*, vol. 29, n° 9, p. 7592-7599, mai 2018, doi: 10.1007/s10854-018-8751-7.

[55] S. Belkhadir *et al.*, « Structural, dielectric and electrocaloric properties of $(Ba_{0.85}Ca_{0.15})(Ti_{0.9}Zr_{0.1-x}Sn_x)O_3$ ceramics elaborated by sol–gel method », *J Mater Sci: Mater Electron*, vol. 30, n° 15, p. 14099-14111, août 2019, doi: 10.1007/s10854-019-01776-1.

[56] P. Kantha *et al.*, « Effect of Sintering Method on the Microstructure and Dielectric Properties of Lead-Free BCZT Ceramics », *AMM*, vol. 866, p. 263-266, juin 2017, doi: 10.4028/www.scientific.net/AMM.866.263.

[57] I. Coondoo *et al.*, « A comparative study of structural and electrical properties in lead-free BCZT ceramics: Influence of the synthesis method », *Acta Materialia*, vol. 155, p. 331-342, août 2018, doi: 10.1016/j.actamat.2018.05.029.

[58] V. S. Puli *et al.*, « Structure, dielectric, ferroelectric, and energy density properties of (1 − x)BZT–xBCT ceramic capacitors for energy storage applications », *J Mater Sci*, vol. 48, n° 5, p. 2151-2157, mars 2013, doi: 10.1007/s10853-012-6990-1.

[59] X. Chen, X. Chao, et Z. Yang, « Submicron barium calcium zirconium titanate ceramic for energy storage synthesised via the co-precipitation method », *Materials Research Bulletin*, vol. 111, p. 259-266, mars 2019, doi: 10.1016/j.materresbull.2018.11.025.

[60] D. Zhan, Q. Xu, D.-P. Huang, H.-X. Liu, W. Chen, et F. Zhang, « Dielectric nonlinearity and electric breakdown behaviors of $Ba_{0.95}Ca_{0.}05Zr_{0.3}Ti_{0.7}O_3$ ceramics for energy storage utilizations », *Journal of Alloys and Compounds*, vol. 682, p. 594-600, oct. 2016, doi: 10.1016/j.jallcom.2016.04.317.

[61] H. Kaddoussi *et al.*, « Sequence of structural transitions and electrocaloric properties in $(Ba_{1-x}Ca_x)(Zr_{0.1}Ti_{0.9})O_3$ ceramics », *Journal of Alloys and Compounds*, vol. 713, p. 164-179, août 2017, doi: 10.1016/j.jallcom.2017.04.148.

[62] G. Singh, V. S. Tiwari, et P. K. Gupta, « Electro-caloric effect in $(Ba_{1-x}Ca_x)(Zr_{0.05}Ti_{0.95})O_3$: A lead-free ferroelectric material », *Appl. Phys. Lett.*, vol. 103, n° 20, p. 202903, nov. 2013, doi: 10.1063/1.4829635.

[63] M. Sanlialp, V. V. Shvartsman, M. Acosta, B. Dkhil, et D. C. Lupascu, « Strong electrocaloric effect in lead-free $0.65Ba(Zr_{0.2}Ti_{0.8})O_3$ -$0.35(Ba_{0.7}Ca_{0.3})TiO_3$ ceramics obtained by direct measurements », *Appl. Phys. Lett.*, vol. 106, n° 6, p. 062901, févr. 2015, doi: 10.1063/1.4907774.

[64] J. Wang, T. Yang, S. Chen, G. Li, Q. Zhang, et X. Yao, « Nonadiabatic direct measurement electrocaloric effect in lead-free $Ba,Ca(Zr,Ti)O_3$ ceramics », *Journal of Alloys and Compounds*, vol. 550, p. 561-563, févr. 2013, doi: 10.1016/j.jallcom.2012.10.144.

[65] S. Patel, A. Chauhan, et R. Vaish, « Enhanced electrocaloric effect in Fe-doped $(Ba_{0.85}Ca_{0.15}Zr_{0.1}Ti_{0.9})O_3$ ferroelectric ceramics », *Applied Materials Today*, vol. 1, n° 1, p. 37-44, nov. 2015, doi: 10.1016/j.apmt.2015.08.002.

[66] B. Asbani *et al.*, « Lead-free $Ba_{0.8}Ca_{0.2}(Zr_xTi_{1-x})O_3$ ceramics with large electrocaloric effect », *Appl. Phys. Lett.*, vol. 106, n° 4, p. 042902, janv. 2015, doi: 10.1063/1.4906864.

Table captions

Table. 1. Structural parameters, average crystalline size, average grain size and relative density of BCZT ceramics sintered at different dwell times.

Table. 2. Dielectric properties of BCZT ceramics performed at 1 kHz.

Table. 3. Comparison of dielectric and ferroelectric properties of BCZT ceramics in the present work with others reported in the literature for various synthesis methods and sintering conditions.

Table. 4. Comparison of energy storage properties of the BCZT family ceramics.

Table. 5. Comparison of the ECE properties of BCZT ceramics with other lead-free materials reported in the literature.

Figure captions

Fig.1. XRD patterns and Rietveld refinement of BCZT samples sintered for various dwell times : (a) 2h, (b) 4h, (c) 6h and (d) & (e) XRD patterns around $44° < 2\theta < 46°$ and $65° < 2\theta < 67°$ of BCZT ceramics.

Fig.2. SEM micrographs and grain size distributions with Gaussian fitting (inset) of the samples sintered at various dwell times: (a) 2h, (b) 4h and (c) 6h.

Fig.3. EDX spectra of BCZT ceramic sintered for 4h.

Fig.4. Temperature variation of dielectric properties of BCZT samples measured at 1 kHz and sintered at various sintering times.

Fig.5. Temperature dependence of dielectric permittivity at different frequencies of BCZT samples sintered for 4h. Inset: derivative of relative dielectric permittivity as a function of temperature.

Fig.6. Curie–Weiss fitting curves of BCZT samples sintered for 4h.

Fig. 7. P-E hysteresis loops of the BCZT samples sintered for 4h.

Fig. 8. Room-temperature P–E curves of the BCZT samples.

Fig. 9. P–E curve of the BCZT-4h at 140 °C with a schematic for calculating energy storage performance.

Fig. 10. Energy-storage properties of the BCZT samples as a function of sintering time.

Fig. 11. Temperature profiles of the electrocaloric temperature change (ΔT) for various sintering times at 6 kV/cm applied electric field.

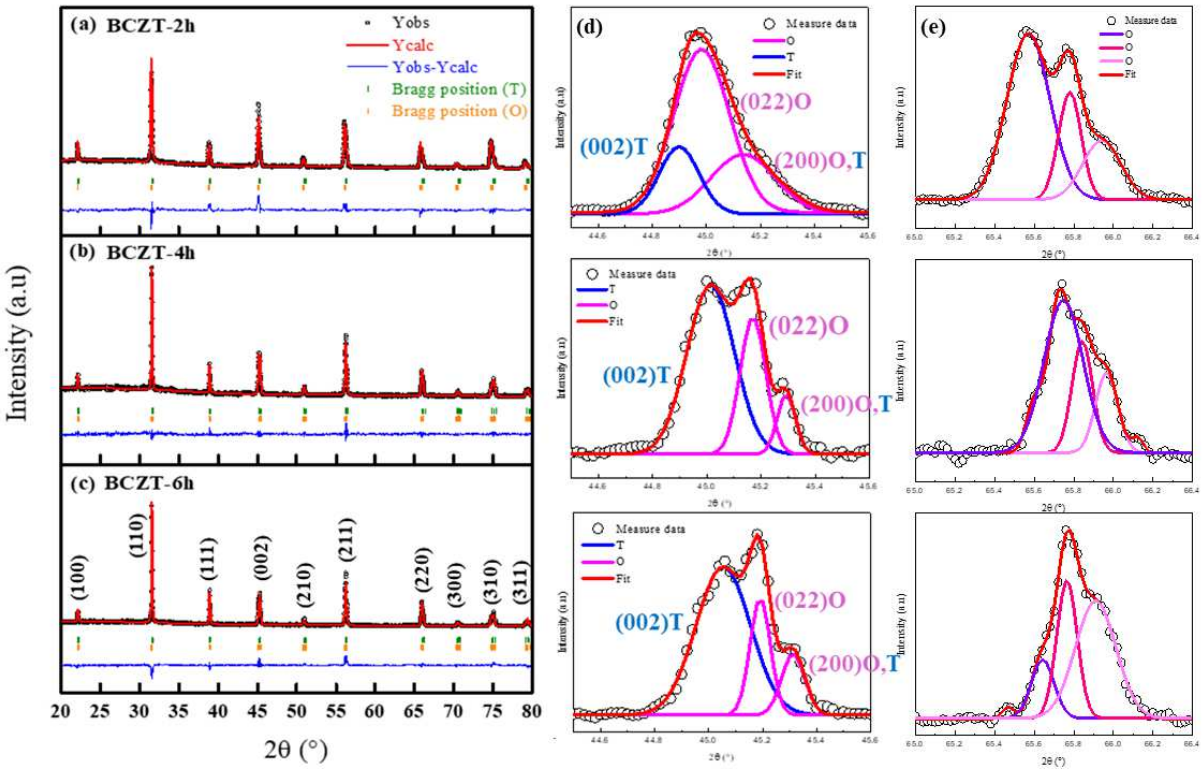
(a) BCZT-2h
Yobs
Ycalc
Yobs-Ycalc
Bragg position (T)
Bragg position (O)
(b) BCZT-4h
(c) BCZT-6h
(100)
(110)
(111)
(002)
(210)
(211)
(220)
(300)
(310)
(311)
Intensity (a.u)
2θ (°)
(d)
(e)
Measure data
O
T
Fit
(022)O
(002)T
(200)O,T

Fig.1.

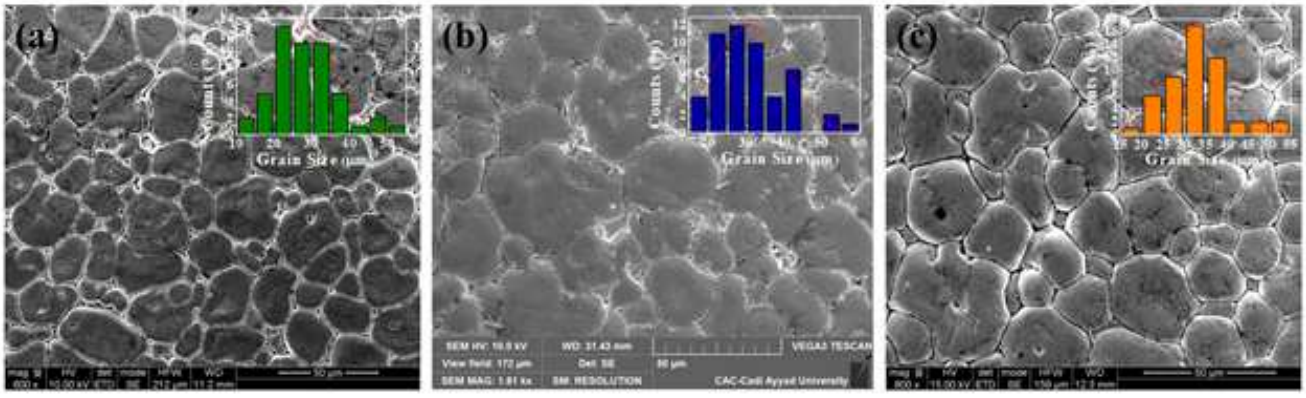
(a)
(b)
(c)
Grain Size (μm)

Fig.2.

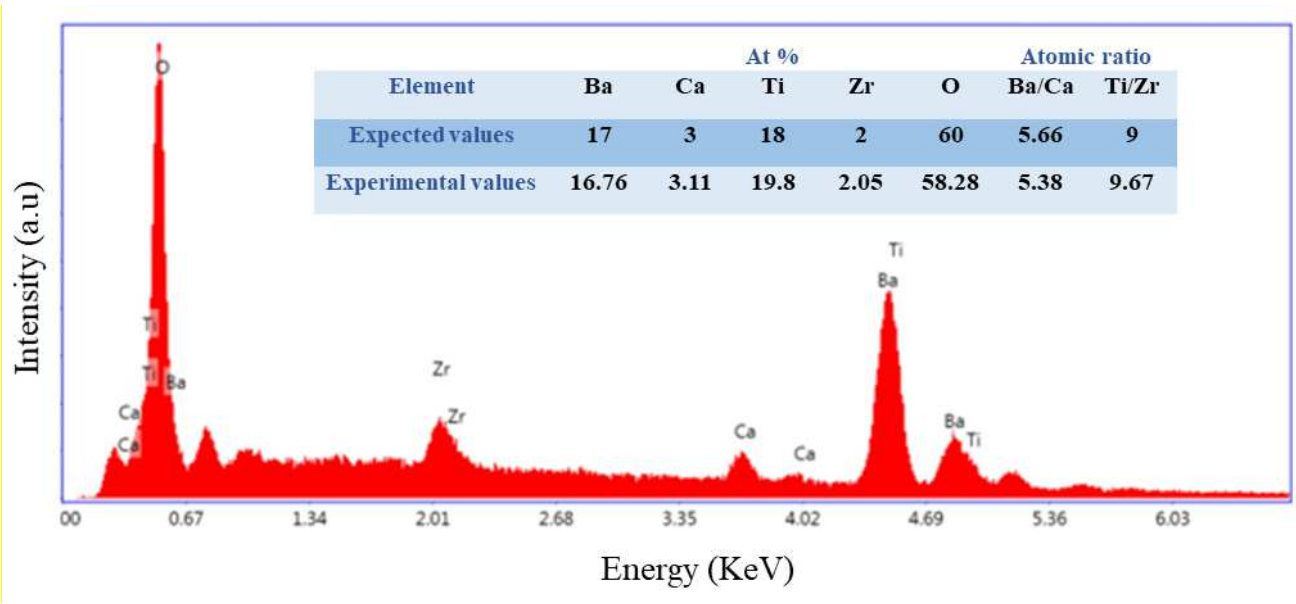
At %
Atomic ratio
Element | Ba | Ca | Ti | Zr | O | Ba/Ca | Ti/Zr
Expected values | 17 | 3 | 18 | 2 | 60 | 5.66 | 9
Experimental values | 16.76 | 3.11 | 19.8 | 2.05 | 58.28 | 5.38 | 9.67
Intensity (a.u)
Energy (KeV)
O
Ti
Ba
Ca
Zr
00
0.67
1.34
2.01
2.68
3.35
4.02
4.69
5.36
6.03

Fig.3.

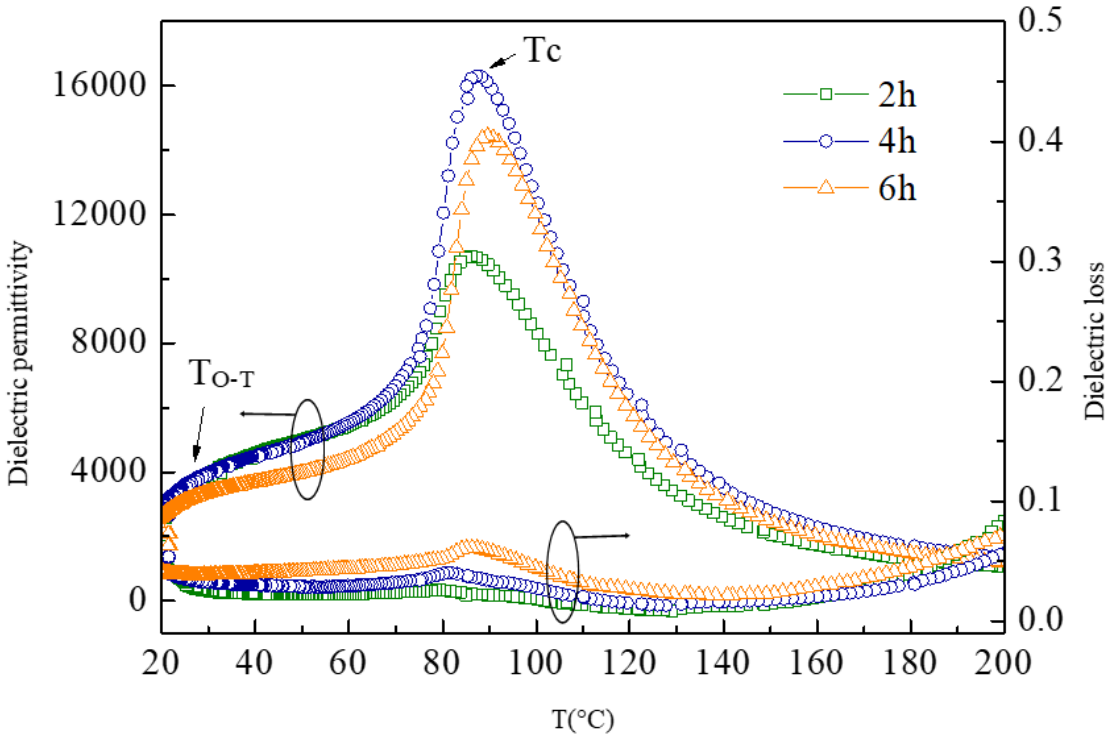
Tc
To-T
2h
4h
6h
Dielectric permittivity
Dielectric loss
T(°C)
16000
12000
8000
4000
0
0.5
0.4
0.3
0.2
0.1
0.0
20
40
60
80
100
120
140
160
180
200

Fig.4.

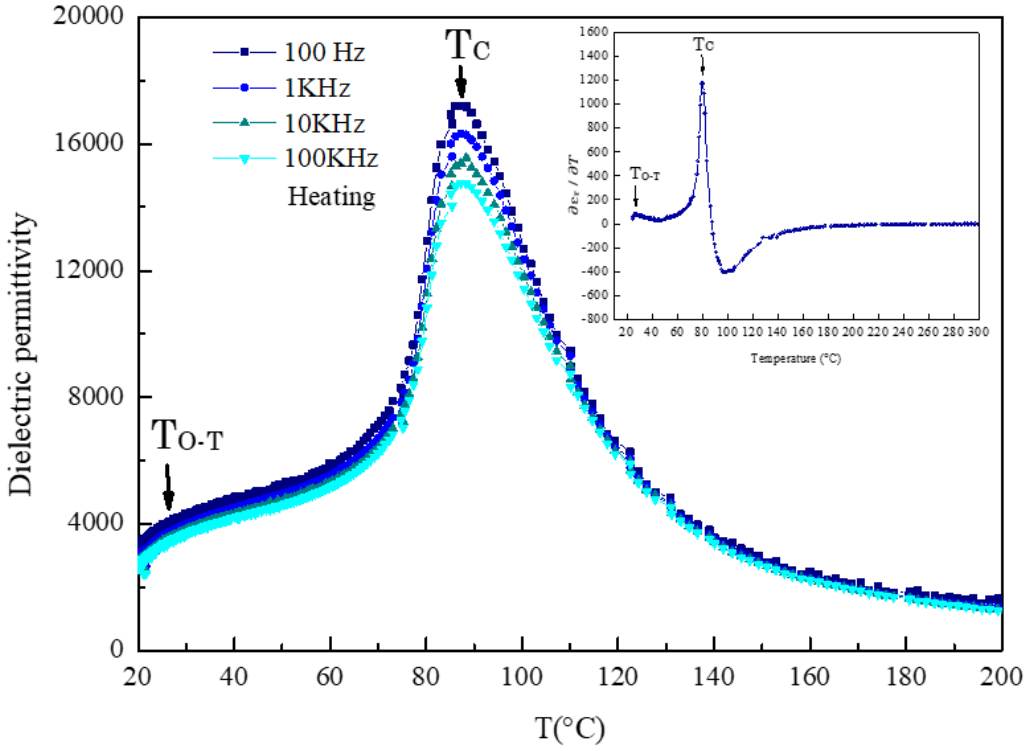
100 Hz
1KHz
10KHz
100KHz
Heating
Tc
To-T
Dielectric permittivity
T(°C)
Temperature (°C)

Fig.5.

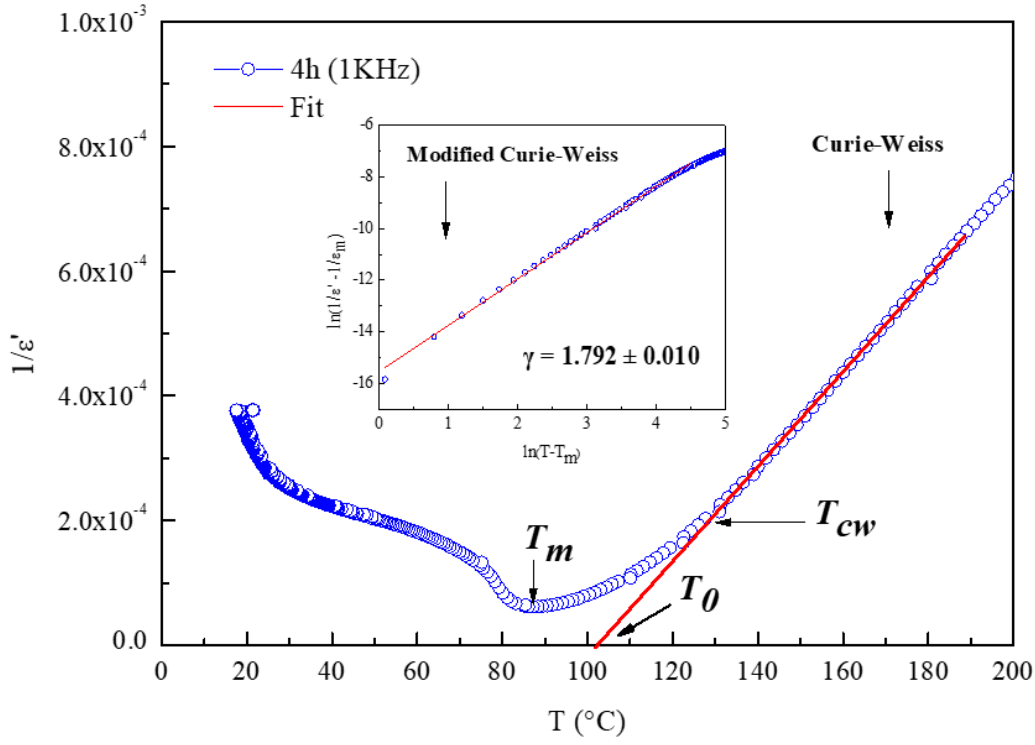
4h (1KHz)
Fit
Modified Curie-Weiss
Curie-Weiss
γ = 1.792 ± 0.010
Tm
T0
Tcw
1/ε'
T (°C)

Fig.6.

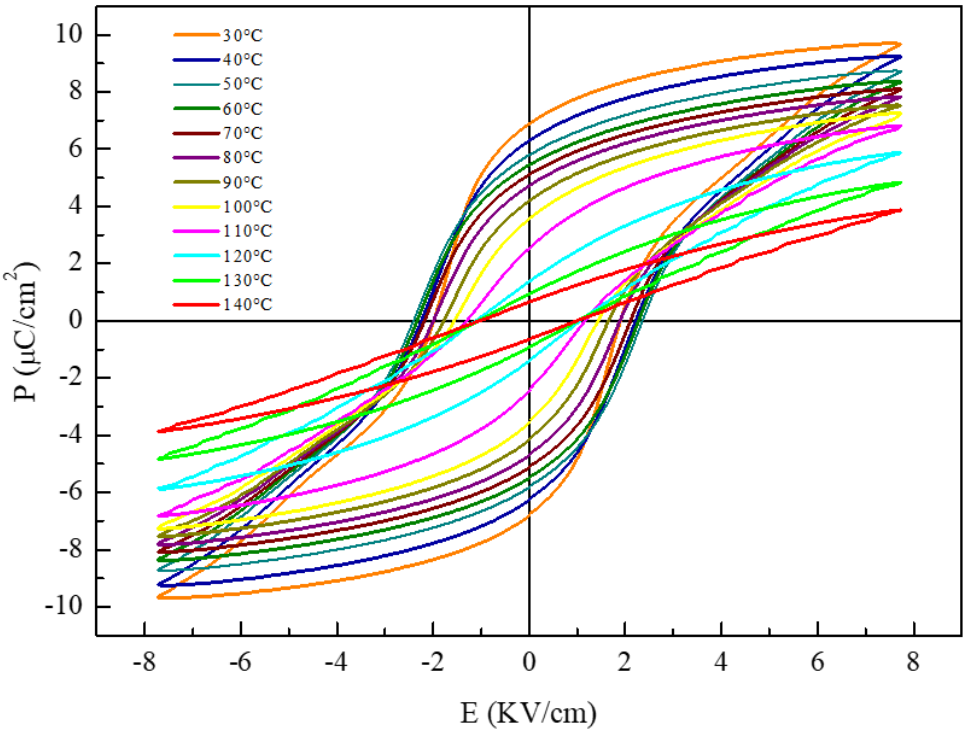
30°C
40°C
50°C
60°C
70°C
80°C
90°C
100°C
110°C
120°C
130°C
140°C
P (μC/cm²)
E (KV/cm)

Fig. 7.

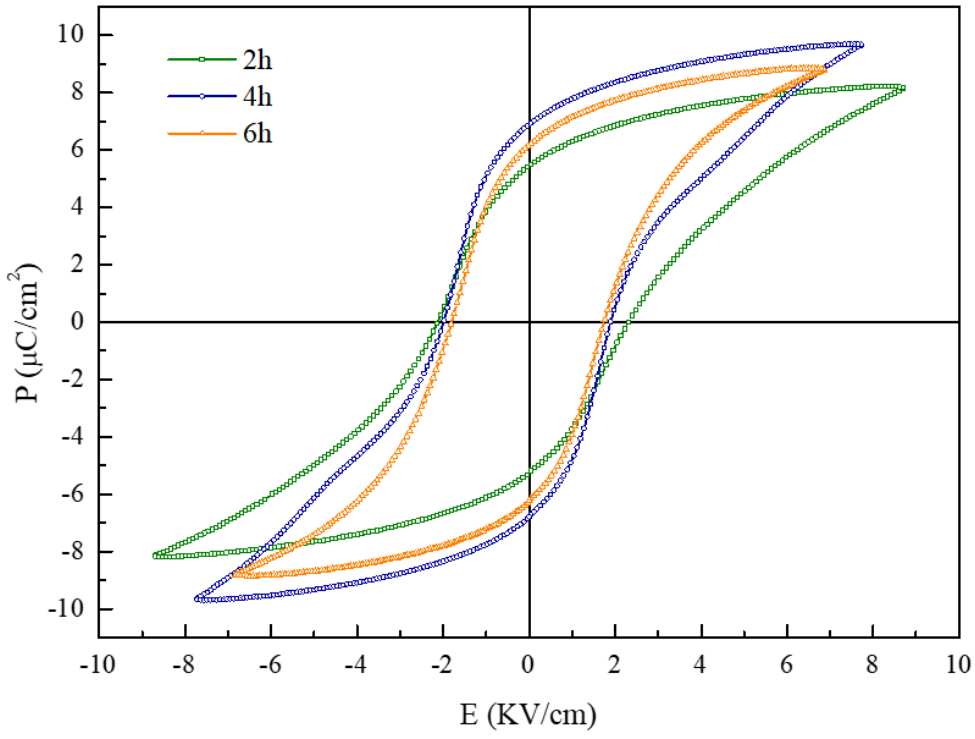
2h
4h
6h
P (μC/cm²)
E (KV/cm)

Fig. 8.

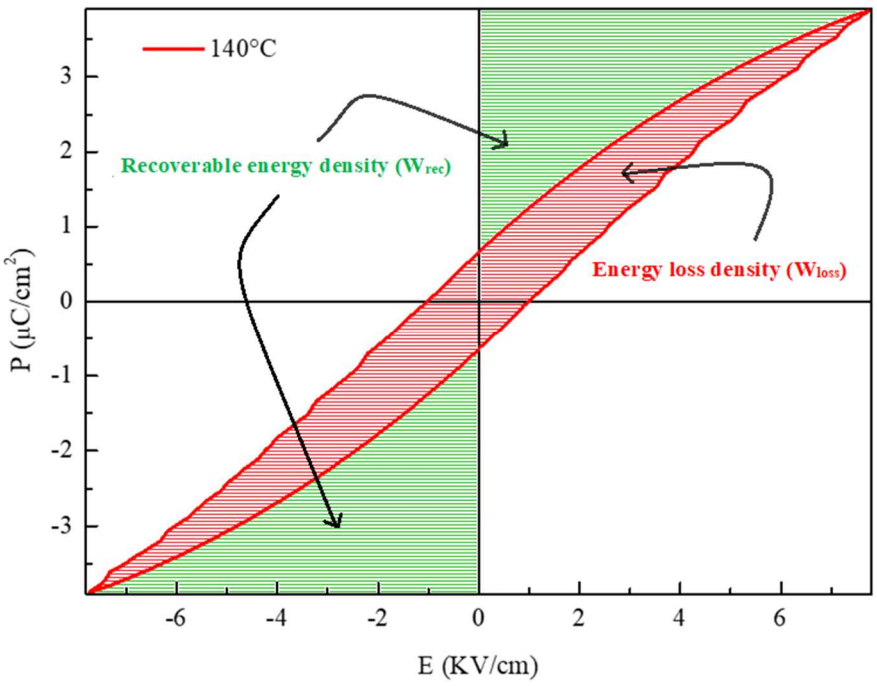
140°C
Recoverable energy density (Wrec)
Energy loss density (Wloss)
P (μC/cm2)
E (KV/cm)

Fig. 9.

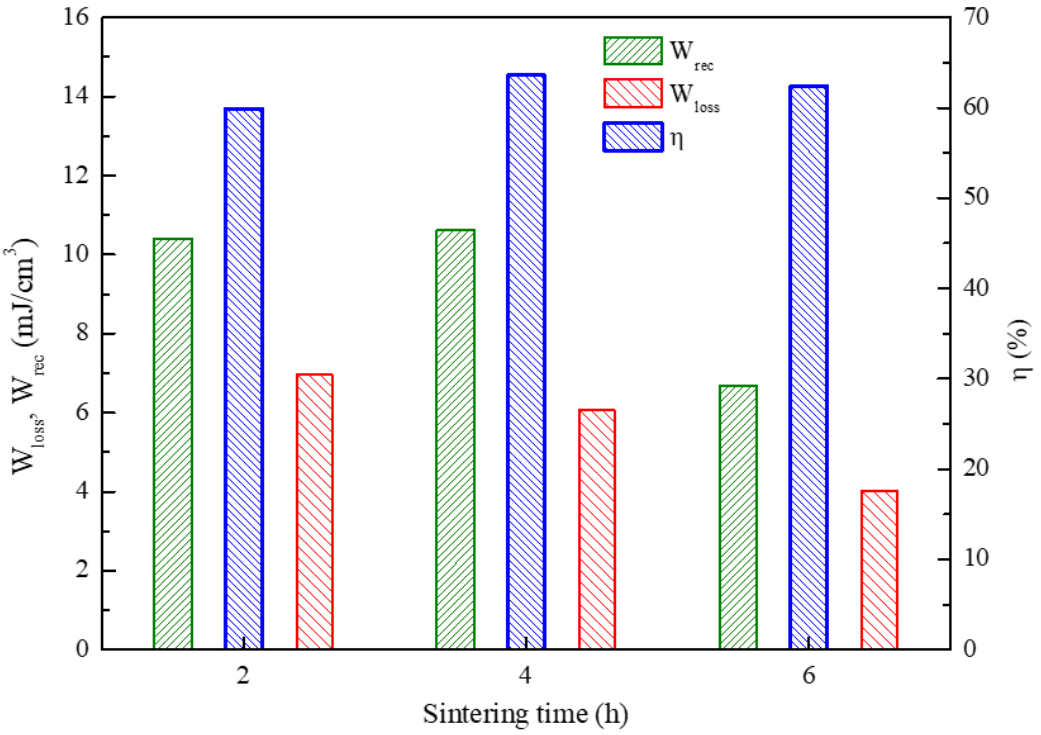
Wrec
Wloss
η
Wloss, Wrec (mJ/cm3)
η (%)
Sintering time (h)

Fig. 10.

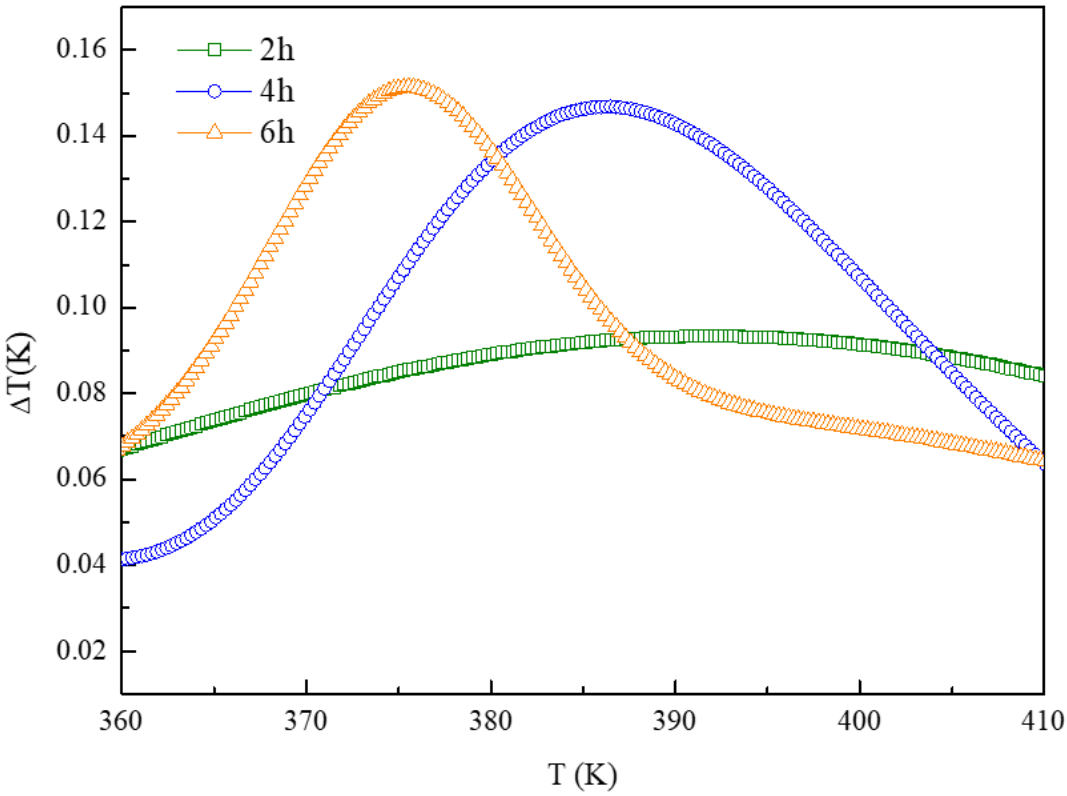
2h
4h
6h
0.16
0.14
0.12
0.10
0.08
0.06
0.04
0.02
ΔT(K)
360
370
380
390
400
410
T (K)

Fig. 11.

Table. 1.

Sintering time (h)	Structure	Unit cell parameters				Tetragonality (c/a)	Phase compositions (wt%)	Reliability factors (%)			Average crystalline size (nm) by XRD	Average grain size(μm) by SEM	Relative density (%)
		a(Å)	b(Å)	c(Å)	V (Å^3)			Rwp	Rp	χ^2			
2	Tetragonal	3.9989	3.9989	4.0053	64.052	1.0016	55.92	24.3	33.8	0.88	24.96	28.04	94.5
	+												
	Orthorhombic	4.0188	4.0130	4.0144	64.744		44.08						
4	Tetragonal	3.9928	3.9928	4.0092	63.918	1.0041	77.52	27.8	42.5	1.06	32.95	30.79	98.5
	+												
	Orthorhombic	3.9957	4.0134	4.0053	64.231		22.48						
6	Tetragonal	3.9988	3.9988	4.0122	64.159	1.0033	60.60	27.6	35.7	0.94	33.80	33.23	97.8
	+												
	Orthorhombic	4.0162	3.9952	4.0073	64.300		39.40						

Table. 2.

Sintering time (h)	$\varepsilon_{r,max}$ at 1kHz	$\tan\delta_{max}$ at 1kHz	T_{O-T} (°C)	T_m (°C)	T_0 (°C)	T_{cw} (°C)	ΔT_m (°C)	$C \times 10^5$ (°C)	γ
2	10704	0,025	31	86.20	98.67	125.94	39.74	1.052	1.760
4	16310	0,040	27	87.22	102.61	128.11	40.89	1.302	1.792
6	14439	0,060	24	89.60	104.39	129.53	39.93	1.118	1.783

Table. 3.

Sintering regime (°C-h)	Synthesis method	Average grain size(μm)	Relative density (%)	$\varepsilon_{r,max}$	$\tan\delta_{max}$	R_{sq}	Ps ($\mu C/cm^2$)	Pr ($\mu C/cm^2$)	Ec (kV/cm)	E (kV/cm)	Refs
1420-2	Sol-gel	28.04	94.5	10704	0,025	1.9653	8.2134	5.4410	2.3131	8.75	This work
1420-4	Sol-gel	30.79	98.5	16310	0,040	1.9295	9.6955	6.8854	1.8979	7.77	This work
1420-6	Sol-gel	33.23	97.8	14439	0,060	1.9424	8.8492	6.1749	1.7427	6.89	This work
1400-2	Sol-gel	---	95	8808	0.02	---	18	12.24	2.66	30	[54]
1420-6	Sol-gel	---	----	16480	0.015	---	17.76	11.64	1.78	30	[19]
1350-2	Sol-gel	1.5	---	6500	0.2	---	3	0.7	1.9	12	[55]
1450-2	Sol-gel	3	81	6800	---	---	15	4.5	2.61	50	[47]
1550-2	Sol-gel	10	97	20200	---	---	20	10.7	1.85	40	[47]
1400-2	Sol-gel-hydrothermal	---	95	9173	---	---	42	12.56	≈2.16	40	[33]
1300-3	Hydrothermal	12.09	---	7760	0.1	---	25	10.835	2.265	15	[41]
1500-4	Solid state	32.2	97.2	16300	0.017	---	24	12	5	55	[10]
1500-2	Solid state	20.8	---	9926	0.0108	---	---	---	---	---	[56]
1300-3	Solid state	27.61	95	4500	0.12	---	13.8	10.8	5.8	30	[57]

Table. 4.

Material	Sintering regime (°C-h)	Synthesis method	W_{rec} (mJ/cm^3)	W_{loss} (mJ/cm^3)	η (%)	E (kV/cm)	ESV (%)	Refs
$Ba_{0.85}Ca_{0.15}Zr_{0.1}Ti_{0.9}O_3$	1420-2	Sol-gel	10.40	6.96	59.90	8.75	25.07	This work
$Ba_{0.85}Ca_{0.15}Zr_{0.1}Ti_{0.9}O_3$	1420-4	Sol-gel	10.61	6.06	63.65	7.77	19.87	This work
$Ba_{0.85}Ca_{0.15}Zr_{0.1}Ti_{0.9}O_3$	1420-6	Sol-gel	6.66	4.02	62.36	6.89	28.88	This work
$Ba_{0.85}Ca_{0.15}Zr_{0.1}Ti_{0.9}O_3$	1420-6	Sol-gel	520	---	---	30	---	[19]
$Ba_{0.85}Ca_{0.15}Zr_{0.1}Ti_{0.9}O_3$	1420-6	Solid state	310	---	---	30	---	[19]
$[(BaZr_{0.2}Ti_{0.80})O_3]_{0.85}$ $[(Ba_{0.70}Ca_{0.30})TiO_3)]_{0.15}$	1600-4	Solid state	940	680	72	170	---	[58]
$Ba_{0.85}Ca_{0.15}Zr_{0.1}Ti_{0.9}O_3$	1320-6	Co-precipitation	250	130	65	100	---	[59]
$Ba_{0.95}Ca_{0.05}Zr_{0.3}Ti_{0.7}O_3$	1280-2	Citrate method	590	---	72.8	160	---	[60]
$Ba_{0.85}Ca_{0.15}Zr_{0.1}Ti_{0.9}O_3$	1250-10	Hydrothermal	367.2	178.9	67.2	60	12.7	[49]
$0.6BaZr_{0.20}Ti_{0.80}O_3$–$0.4Ba_{0.70}Ca_{0.30}TiO_3$	1250-3	Solid state	121	52	70	25	46.3	[50]

Table. 5.

Material	Sintering regime (°C-h)	$FWHM_{\Delta T}$ (K)	$\Delta T_{EC,max}$ (K)	ΔE (kV/cm)	ξ (K mm/kV)	Synthesis method	Measurement method	Refs
$Ba_{0.85}Ca_{0.15}Zr_{0.1}Ti_{0.9}O_3$-2h	1420-2	56	0.0933	6	0.155	Sol-gel	Indirect	Present work
$Ba_{0.85}Ca_{0.15}Zr_{0.1}Ti_{0.9}O_3$-4h	1420-4	33	0.1467	6	0.244	Sol-gel	Indirect	Present work
$Ba_{0.85}Ca_{0.15}Zr_{0.1}Ti_{0.9}O_3$-6h	1420-6	23	0.1513	6	0.252	Sol-gel	Indirect	Present work
$Ba_{0.85}Ca_{0.15}Zr_{0.1}Ti_{0.9}O_3$	1350-2	---	0.0150	6	0,025	Sol-gel	Indirect	[55]
$Ba_{0.85}Ca_{0.15}Zr_{0.1}Ti_{0.9}O_3$	1420-2	---	0.1520	8	0.190	Solid state	Indirect	[61]
$Ba_{0.8}Ca_{0.2}Zr_{0.06}Ti_{0.94}O_3$	1420-2	---	0.2100	7.95	0.264	Solid state	Indirect	[62]
$0.65Ba(Zr_{0.2}Ti_{0.8})O_3$-$0.35(Ba_{0.7}Ca_{0.3})TiO_3$	1500-2	---	0.3300	20	0.165	Solid state	Direct	[63]
$Ba_{0.98}Ca_{0.02}(Zr_{0.085}Ti_{0.915})O_3$	1280-2	---	0.6000	40	0.150	Solid state	Direct	[64]
$Ba_{0.85}Ca_{0.15}Zr_{0.1}Ti_{0.9}O_3$	1400-4	---	0.4000	21.5	0.186	Solid state	Indirect	[65]
$Ba_{0.8}Ca_{0.2}Zr_{0.04}Ti_{0.96}O_3$	1350-2	---	0.2700	7.95	0.340	Solid state	Indirect	[66]